JORDAN JOURNAL OF BIOLOGICAL SCIENCES

Jordan Journal of Biological Sciences

Journal homepage: www.jjbsci.com

Synergizing Traditional Medicine and Computational Biology to Explore SGTP1 Inhibition by Triphala Churna Phytochemicals in Schistosomiasis through Molecular and Biophysical Approaches

Mounica Subhaprada Goodala[1], Nidheesh L B[1], Deekshitha M[1]

[1] Department of Bioinformatics, BioNome, Bengaluru, Karnataka, India-560043.

To cite this article: Mounica Subhaprada Goodala, Nidheesh L B, Deekshitha M(2026) Synergizing Traditional Medicine and Computational Biology to Explore SGTP1 Inhibition by Triphala Churna Phytochemicals in Schistosomiasis through Molecular and Biophysical Approaches; JJBS; 18:1, 25:45.

Corresponding author:

Deekshitha M

Department of Bioinformatics, BioNome, Bengaluru, Karnataka, India-560043

Email: info@bionome.in

ORCID:

Mounica Subhaprada Goodala: https://orcid.org/0009-0001-9242-2774

Nidheesh L B: https://orcid.org/0009-0005-7973-6137

ABSTRACT

Schistosomiasis remains a pervasive neglected tropical disease, afflicting over 250 million individuals globally, with significant limitations in current therapeutic interventions, including praziquantel, which fails to target juvenile parasites or prevent reinfections. This study sought to explore phytochemical inhibitors of Schistosome Glucose Transporter Protein 1 (SGTP1), a critical facilitator of parasite survival, leveraging the bioactive potential of compounds derived from the Ayurvedic formulation Triphala churna. The research employed molecular docking using AutoDock Vina to evaluate binding affinities, followed by pharmacokinetic analysis with SwissADME and ProTox-II for absorption, distribution, metabolism, excretion, and toxicity profiling. Arjunolic acid, with a docking score of -9.8 kcal/mol, showed the most robust binding to SGTP1. Toxicity evaluations indicated its safety, with a non-toxic profile, high GI absorption, and no inhibitory effects on major cytochrome P450 enzymes. Molecular dynamics simulations performed with GROMACS further validated its interaction stability with SGTP1, exhibiting low RMSD (~1.8 Å) and RMSF values, consistent hydrogen bonding, and stable solvent-accessible surface area. The principal component analysis reinforced the suitability of arjunolic acid as an SGTP1 inhibitor. Results highlight arjunolic acid's superior pharmacological profile and binding efficiency, distinguishing it as a promising candidate for disrupting schistosome glucose uptake mechanisms. Its non-toxic nature and stability under dynamic conditions provide a strong rationale for advancing to experimental validations. This study demonstrates the efficacy of integrating traditional medicine with computational tools to identify sustainable therapeutic candidates for schistosomiasis. Future perspectives include in vitro and in vivo studies to validate arjunolic acid's inhibitory effects, potentially leading to novel treatments addressing the limitations of current therapies.

Keywords: *Arjunolic acid, Schistosomiasis, SGTP1 Inhibition, Molecular Docking, Pharmacokinetics, Molecular Dynamics Simulation, Traditional Medicine, omputational Drug Design*

ARTICLE HISTORY

Received 06 Jan 2026
Accepted 27 Jan 2026

INTRODUCTION

Schistosomiasis, a parasitic disease caused by trematodes of the genus *Schistosoma*, remains a significant global health challenge, disproportionately affecting impoverished communities [1]. This neglected tropical disease (NTD) afflicts over 250 million people worldwide, with more than 85% of the burden concentrated in sub-Saharan Africa. It is prevalent in regions with inadequate sanitation, limited healthcare, and poor access to safe water, perpetuating its transmission through freshwater habitats. Schistosomiasis is responsible for an estimated annual loss of 1.5 to 2.5 million disability-adjusted life years (DALYs) and accounts for approximately 24,000 deaths annually [2, 3]. The lifecycle of *Schistosoma* involves freshwater snails as intermediate hosts, releasing free-swimming larvae, or cercariae, which penetrate human skin upon contact. Chronic infection is characterized by egg deposition in tissues, leading to granuloma formation, chronic inflammation, and severe complications such as liver fibrosis, kidney failure, and bladder cancer. Despite mass drug administration (MDA) programs using praziquantel (PZQ) to control morbidity, reinfection, resistance concerns, and the inability of PZQ to target juvenile worms underscore the urgent need for alternative therapeutic interventions [4].

The glucose metabolism of *Schistosoma* represents an essential pathway for the parasite's survival and pathogenicity. Glucose is a vital energy source for the parasite, enabling its growth, reproduction, and energy-intensive lifecycle. The *Schistosoma* Glucose Transporter Protein 1 (SGTP1) plays a pivotal role in the uptake and intracellular transport of glucose [5]. Studies reveal that adult *Schistosoma* consume approximately 20% of their dry weight in glucose per hour, relying on SGTP1 to meet these demands. SGTP1 is expressed across various parasite stages, including cercariae, schistosomula, and adult worms. Its inhibition significantly impairs glucose uptake, reducing parasite viability. This critical role positions SGTP1 as a compelling therapeutic target, especially given the parasite's adaptive mechanisms to increase transporter expression during glucose deprivation. By targeting SGTP1, it may be possible to disrupt the parasite's metabolic pathways, paving the way for novel therapeutic approaches that extend beyond the limitations of current interventions [5, 6].

The quest for new therapeutic agents has increasingly turned to natural products, particularly those derived from traditional medicine systems such as Ayurveda. Ayurvedic formulations, deeply rooted in Indian medicinal traditions, often involve polyherbal combinations designed to harness synergistic effects among individual components [7]. Polyherbal formulations are known for their ability to enhance therapeutic efficacy while minimizing adverse effects, making them a cornerstone of Ayurvedic treatment. Among these, Triphala churna is one of the most prominent and extensively studied formulations. Composed of three botanicals—*Terminalia bellirica*, *Terminalia chebula*, and *Emblica officinalis*—Triphala churna has demonstrated a broad spectrum of pharmacological properties. [8] These include antioxidant, immunomodulatory, anti-inflammatory, hypoglycemic, and antiglycation activities. Its traditional applications span detoxification, rejuvenation, and treatment of metabolic disorders [9], highlighting its potential utility in conditions

requiring glucose regulation, such as Schistosomiasis.

While natural products such as Triphala churna hold great promise, their systematic evaluation for specific therapeutic purposes has often been limited by a lack of robust scientific validation. Computational methods have revolutionized the drug discovery process, offering powerful tools for identifying and validating bioactive compounds in silico. Molecular docking enables the prediction of interactions between phytocompounds and biological targets, such as SGTP1, while molecular dynamics simulations provide insights into the stability, conformational changes, and energetics of these interactions. These in-silico approaches allow for the rapid screening and refinement of potential drug candidates, significantly reducing the time and cost associated with traditional drug discovery processes [10].

The integration of traditional Ayurvedic wisdom with modern bioinformatics tools offers a unique and innovative approach to addressing the global challenge of Schistosomiasis. The present study aims to investigate the therapeutic potential of phytocompounds derived from Triphala churna against SGTP1, leveraging molecular docking and molecular dynamics simulations. By targeting the glucose transport mechanism essential for *Schistosoma* survival, this research seeks to bridge the gap between traditional medicine and modern therapeutics, contributing to the development of novel, cost-effective, and sustainable solutions for Schistosomiasis control. The reliance of *Schistosoma* on glucose transport for survival presents a strategic vulnerability that can be exploited for therapeutic purposes. Triphala churna, with its rich pharmacological profile, represents a promising source of bioactive compounds that can be systematically evaluated through advanced computational techniques. The findings of this study have the potential to open new avenues for plant-based anti-schistosomal therapies, addressing the limitations of existing treatments and advancing global efforts towards the elimination of Schistosomiasis.

Materials and Methods

1.1. Retrieval of SGTP1 Protein Sequence

The FASTA sequence of *Schistosoma mansoni* Glucose Transport Protein 1 (SGTP1) was retrieved from the NCBI database (GenBank Accession: AAA19732.1), accessed on 24th August 2024 (https://www.ncbi.nlm.nih.gov/). NCBI is a reliable repository for biological data, providing access to genomic and protein sequences essential for bioinformatics studies. SGTP1, a critical protein involved in glucose uptake, was selected as the therapeutic target for the downstream analyses.

1.2. Homology Modeling and Validation of SGPT1

Homology modeling of *Schistosoma mansoni* Glucose Transporter Protein 1 (SGTP1) was performed using the SWISS-MODEL platform, a widely used web-based tool for comparative protein structure prediction (https://swissmodel.expasy.org/). SWISS-MODEL operates through a streamlined four-step pipeline: identification of structural templates, sequence alignment, model construction, and quality evaluation. This process integrates ProMod3, a robust comparative modeling engine, which extracts initial structural information from templates and resolves insertions and deletions through a combination of database searches and Monte Carlo techniques. Side-chain conformations are modeled using a backbone-dependent rotamer library, and final structural refinements are performed using OpenMM with the CHARMM22/CMAP force field. The modeling process was carried out in Alignment Mode, allowing direct use of a pre-selected template, bypassing the automated template search. The template used, Q26580.1.A, was sourced from the AlphaFold DB and corresponds to the glucose transport protein of *Schistosoma mansoni* (Gene: GTP2) with 100% sequence identity. This high-quality template ensured accurate alignment and reliable structural predictions [11].

The modeled structure of SGTP1 was validated using the Ramachandran plot, MolProbity, and QMEAN (Qualitative Model Energy ANalysis) local scores, ensuring its structural accuracy. The Ramachandran plot assessed backbone φ (phi) and ψ (psi) torsion angles, categorizing residues into favorable regions to confirm stereochemical quality. MolProbity evaluated atomic model quality, identifying steric clashes and geometric inconsistencies to refine the model. QMEAN (Qualitative Model Energy ANalysis) local scores provided residue-specific reliability by comparing predicted atomic interactions with experimental data, highlighting well-modeled regions and areas requiring refinement [12].

1.3. Normal Mode Analysis

Normal Mode Analysis (NMA) was conducted to investigate the intrinsic dynamics and collective motions of the SGTP1. NMA (https://imods.iqf.csic.es/) is a powerful computational technique used in bioinformatics to explore the vibrational modes of biomolecular frameworks, providing insights into structural flexibility and functional dynamics. This method approximates the potential energy landscape of a biomolecule using a harmonic oscillator model, enabling the study of vibrational frequencies and significant normal modes through linear algebra techniques [13]. These modes represent collective atomic motions within the protein, which are often associated with biological activities such as ligand binding, enzymatic function, and allosteric regulation. In this study, NMA was performed using the iMODS server, a robust platform for modeling and visualizing protein dynamics. The harmonic potential approximation in iMODS simplifies complex molecular interactions, allowing for the identification of critical vibrational modes. These modes highlight the collective movements that underlie the functional properties of SGTP1, such as its ligand-binding capabilities [14]. Furthermore, the analysis enabled the visualization of conformational changes and dynamic properties critical to the protein's biological role. The iMODS platform also facilitated the assessment of potential structural changes due to ligand binding, providing predictions on how these interactions might affect SGTP1's stability and dynamics.

1.4. Retrieval of Triphala Churna Phytocompounds

Triphala churna, a renowned Ayurvedic polyherbal formulation comprising *Terminalia bellirica*, *Terminalia chebula*, and *Emblica officinalis*, was analyzed to document its phytochemical constituents. The phytocompounds from these plants were initially identified using the Indian Medicinal Plants, Phytochemistry and Therapeutics (IMPPAT) database (https://cb.imsc.res.in/imppat/home), a comprehensive resource for bioactive molecules in Indian medicinal plants. Duplicate entries were systematically removed to ensure a unique dataset for downstream analysis. The structural data for the shortlisted phytocompounds were subsequently retrieved from the PubChem database (https://pubchem.ncbi.nlm.nih.gov/), a widely recognized repository of chemical information, ensuring high-quality, standardized molecular structures for computational studies. This dataset formed the basis for subsequent downstream analyses [15].

1.5. Virtual Screening of Triphala Churna Phytocompounds against SGPT1

In the present study, molecular docking was conducted to evaluate the interactions between phytocompounds from Triphala churna and the SGTP1 target. Docking simulations were performed using PyRx 0.8 software (https://pyrx.sourceforge.io/), which integrates AutoDock Vina and OpenBabel for virtual screening and energy minimization. The SGTP1 protein structure was prepared by removing non-structural components, such as water molecules, and assigning Kollman charges and AD4 atom types to all macromolecular receptor atoms in DS Biovia Discovery Studio. The prepared protein was then converted into pdbqt format for compatibility with AutoDock Vina in PyRx [15].

The phytocompounds selected for docking were optimized by consolidating nonbonded atoms, defining torsional angles, and performing energy minimization using the universal force field (UFF) available in PyRx. The optimized ligands were converted into pdbqt format using OpenBabel to ensure compatibility with the docking software. Docking simulations were conducted by generating multiple conformational poses of the ligands within SGTP1's binding pocket, identified using the grid box parameters: center_x = -1.05, center_y = -0.7382, center_z = 3.8243, with dimensions size_x = 67.82, size_y = 58.23, and size_z = 92.28. Exhaustiveness was set to 8 for optimal sampling of ligand binding conformations. The binding affinities of the docked complexes were ranked based on kcal/mol values at zero Root Mean Square Deviation (RMSD) to ensure consistent positioning. Visualization of docked complexes was performed using DS Biovia Discovery Studio to analyze interactions between phytocompounds and SGTP1's amino acid residues [16].

1.6. Binding interactions of Triphala Churna Phytocompounds with SGPT1

Molecular visualization was performed using Biovia Discovery Studio to analyze the interactions between Triphala churna-derived phytocompounds and the SGTP1 target. The top eight docked models with binding scores better than -7 kcal/mol were selected for detailed examination. Visualization enabled the identification of key residues within the binding pocket of SGTP1 and the specific interactions contributing to the stability and binding affinity of the ligand-protein complexes. Interaction types, including hydrogen bonds, hydrophobic interactions, and van der Waals forces, were categorized and evaluated to understand their contribution to the overall binding mechanism. Distances between interacting atoms were measured to confirm and quantify the binding strength, with special emphasis on hydrogen bonding residues, which play a critical role in stabilizing the complexes [15, 16].

1.7. Pharmacokinetic Profiling of Triphala Churna Phytocompounds

The pharmacokinetic properties of the selected Triphala churna phytocompounds were evaluated in silico using the SwissADME webserver (http://www.swissadme.ch/). Early ADME (Absorption, Distribution, Metabolism, and Excretion) predictions during the drug discovery phase significantly reduce the risk of pharmacokinetics-related failures in later stages of drug development. In this study, key molecular and physicochemical descriptors such as molecular weight (MW), molecular refractivity (MR), polar surface area (PSA), lipophilicity, solubility, flexibility, and saturation were calculated using SwissADME [17]. Drug-likeness properties were assessed to estimate the potential of the phytocompounds as oral drug candidates. These assessments were based on established pharmaceutical guidelines, like the Lipinski (Pfizer) rule-of-five, Additionally, the Abbott Bioavailability (BA) score was used to predict the likelihood of achieving at least 10% bioavailability. The phytocompounds' potential interactions with key transport proteins and enzymes were predicted, focusing on their status as substrates or non-substrates for permeability glycoprotein (P-gp) and interactions with cytochrome P450 enzymes. Predictions of gastrointestinal absorption (GIA) and blood-brain barrier (BBB) permeability were included to evaluate pharmacokinetic behavior. Finally, the Pan Assay Interference Compounds (PAINS) filter was applied to identify and exclude any compounds likely to exhibit assay interference properties, ensuring the reliability of the selected candidates for further computational and experimental studies [18].

1.8. Toxicity Profiling

The prediction of compound toxicities plays a crucial role in the drug development process, enabling early identification of safety concerns. Computational toxicity estimations offer significant advantages over traditional methods, providing rapid and cost-effective insights while reducing the need for animal experiments. In the present research, the phytocompounds derived from Triphala churna were subjected to toxicity profiling using the ProTox-II webserver (https://tox.charite.de/protox3/), a robust platform for in silico toxicity prediction [19].

ProTox-II evaluates compound toxicity by leveraging molecular similarity, pharmacophore-based approaches, fragment-based methods, and machine-learning algorithms

trained on extensive toxicological data. The platform predicts acute toxicity using LD50 values, expressed in mg/kg body weight, representing the dose at which 50% of test subjects are expected to succumb to the compound. Additionally, the tool classifies compounds into toxicity categories based on the Globally Harmonized System (GHS) for chemical labeling and classification, ranging from Category 1 (most toxic) to Category 6 (least toxic). By integrating multiple predictive approaches, ProTox-II delivers comprehensive toxicity assessments, including hepatotoxicity, immunotoxicity, carcinogenicity, and mutagenicity [19].

1.9. Molecular Dynamics and Trajectory Analysis

Molecular Dynamics Simulations (MDS) were performed to investigate the stability, conformational flexibility, and binding interactions of the phytocompound Arjunolic acid (PubChem ID: 73641) in complex with SGTP1. MDS is a critical computational technique in drug discovery, providing detailed insights into the dynamic behavior of biomolecules over time, allowing for the evaluation of protein-ligand interactions under near-physiological conditions [20]. By simulating atomic movements based on Newtonian mechanics, MDS captures the intricate dynamics of the system, bridging the gap between static docking predictions and real biological systems.

1.9.1. Simulation Environment and Force Fields

The simulations were performed using the GROMACS 2023.1 software package, known for its efficiency and precision in modeling molecular systems. The CHARMM36 force field was employed to parameterize the SGTP1 protein, while the CHARMM General Force Field (CGenFF) was used for ligand parameterization, ensuring accurate representation of the molecular interactions. The protein-ligand complex, obtained from docking studies, served as the starting structure for the simulation [21].

1.9.2. System Preparation and Equilibration

To mimic physiological conditions, the protein-ligand complex was solvated in a cubic box containing explicit TIP3P water molecules, with counter-ions added to neutralize the system. Energy minimization was performed to eliminate steric clashes and achieve a stable starting conformation. The system was then equilibrated in two phases. First, the NVT ensemble was applied, maintaining constant volume and temperature at 310 K using the velocity-rescaling thermostat to stabilize the kinetic energy distribution. This was followed by the NPT ensemble, where constant pressure at 1 atm and temperature were maintained using the Parrinello-Rahman barostat to replicate physiological thermodynamic conditions accurately [22].

1.9.3. Production Simulation

The production phase involved running a 100-nanosecond simulation under periodic boundary conditions to capture the dynamic behavior of the complex. The simulation employed a time step of 2 femtoseconds, and trajectory snapshots were recorded at regular intervals for post-simulation analysis. The use of periodic boundary conditions eliminated edge effects, while the Verlet cut-off scheme ensured precise calculation of non-bonded interactions [21, 22].

1.9.4. Post-Simulation Trajectory Analysis

Detailed trajectory analyses were performed to evaluate the structural stability and interaction dynamics of the Arjunolic acid (PubChem ID: 73641)-SGPT1 complex. Root Mean Square Deviation (RMSD) was calculated to monitor the overall stability of the protein-ligand complex by tracking conformational changes throughout the simulation. Root Mean Square Fluctuation (RMSF) was used to identify flexible regions within the protein, providing insights into residue-level dynamics. The Radius of Gyration (Rg) was analyzed to assess the compactness and structural integrity of the protein over the simulation timeframe. Hydrogen bond analysis was conducted to evaluate the stability and strength of interactions between the ligand and key residues within the binding pocket. Additionally, Principal Component Analysis (PCA) was performed to explore the dominant motions contributing to the complex's conformational dynamics and the solvent accessible surface area (SASA) was conducted to provide a deeper understanding of the dynamic behavior and stability of the Arjunolic acid (PubChem ID: 73641)-SGPT1 complex [22].

Results

2.1. Modeling of SGPT1 Protein

The three-dimensional structure of Schistosoma mansoni Glucose Transporter Protein 1 (SGTP1) was modeled using the SWISS-MODEL platform with the AlphaFold DB structure of the glucose transport protein (Template: Q26580.1.A) as a reference. The model achieved 100% sequence identity and coverage with the template, resulting in a GMQE score of 0.86, indicating a high-quality predictive structure. The high level of sequence similarity between the target and template underpins the accuracy and reliability of the model, making it a strong candidate for downstream analyses. The structural visualization of SGTP1 (Figure 1a) highlights its helical transmembrane configuration with interspersed random coils and extended strands. This topology, consistent with its functional requirements, underscores its potential as a therapeutic target.

Validation metrics further reinforce the structural accuracy of the model. A MolProbity score of 0.91, coupled with a clash score of 0.77, indicates minimal steric clashes and favorable atomic interactions. The Ramachandran plot revealed 98.37% of residues located in energetically favorable regions, while only 0.20% of residues fell within outlier regions. Such results highlight the stereochemical quality of the model, confirming its suitability for detailed structural and functional studies. Rotamer outliers were minimal, involving residues such as SER, THR, LEU, and ILE, which exhibit minor deviations but do not compromise the global structural integrity. The structure’s predicted monomeric state and transmembrane topology further align with the biological role of SGTP1 as a transporter protein (Figure 1b).

Secondary structure analysis, performed using SOPMA,

revealed that SGTP1 comprises 53.05% alpha helices, 13.21% extended strands, and 33.74% random coils. The high proportion of alpha helices strongly supports the identification of SGTP1 as a transmembrane protein. Alpha helices provide the stability and hydrophobicity required for membrane embedding, while random coil regions add flexibility, enabling interactions with external ligands or other proteins (Figure 1c). The secondary structural elements are crucial for the transporter's functionality, as they facilitate glucose translocation across the lipid bilayer.

Hydropathy analysis using the Kyte-Doolittle scale revealed alternating regions of hydrophobicity and hydrophilicity, characteristic of transmembrane proteins. Hydrophobic regions, largely corresponding to the alpha-helical segments, anchor the protein within the lipid bilayer, while hydrophilic regions, often associated with loops and random coils, interact with the aqueous environment and are likely involved in substrate recognition (Figure 1d). Such structural features align with SGTP1's functional role in glucose uptake, highlighting its critical role in the survival of *Schistosoma mansoni.*

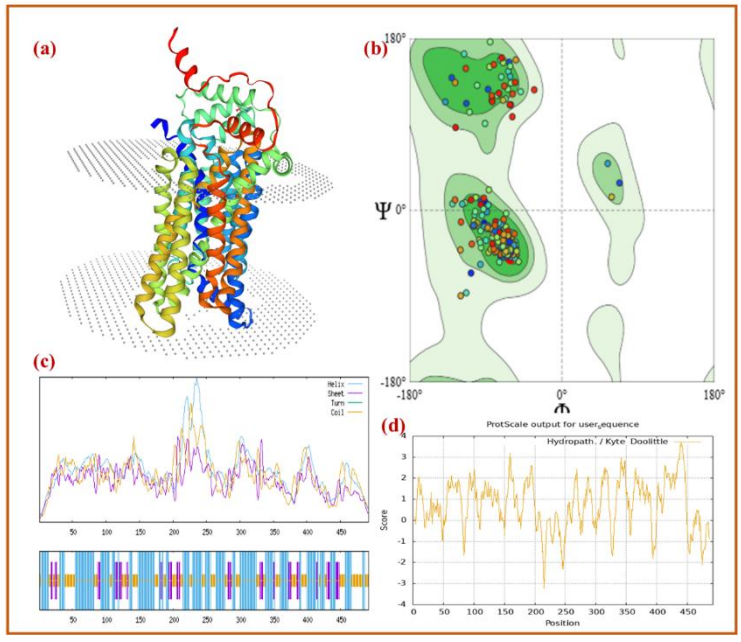

Figure 1. Structural Modeling and Analysis of SGTP1 Protein

(a) The three-dimensional model of SGTP1 depicts the transmembrane configuration of SGTP1, dominated by alpha helices (red and green), with supporting beta strands (yellow) and random coils (blue). This structural arrangement is typical of glucose transporters, enabling their function in glucose translocation across membranes. (b) The Ramachandran plot illustrates the stereochemical quality of the model, with 98.37% of residues occupying favored regions and minimal outliers. (c) The secondary structure composition reveals a high prevalence of alpha helices (53.05%) and significant random coil regions (33.74%), which are crucial for maintaining membrane stability and functional flexibility. (d) The hydropathy plot, generated using the Kyte-Doolittle scale, identifies alternating hydrophobic and hydrophilic regions that correspond to transmembrane domains and solvent-exposed loops, respectively.

2.2. Normal Mode Analysis of SGPT1

The Normal Mode Analysis (NMA) provides a comprehensive understanding of protein dynamics, capturing essential motions that are often linked to biological functions. In this study, NMA of SGTP1 was conducted using the iMODS server, revealing critical insights into its structural stability, flexibility, and correlated residue movements. The results are illustrated in Figure 2, comprising multiple graphical representations that collectively highlight SGTP1's dynamic properties and functional significance.

- ***Structural Flexibility and Deformability***

The deformability graph (Figure 2b) demonstrates the variation in flexibility across different regions of SGTP1, where peaks represent flexible regions and valleys correspond to rigid segments. High deformability was observed at indices 0–50, 200–250, and 400–450, indicating these regions are highly flexible. This flexibility is often associated with functionally critical domains, such as binding sites, active regions, or loop structures, enabling adaptability during substrate interactions or conformational changes. Conversely, indices 50–200 and 250–400 exhibited low deformability, highlighting their role as structural scaffolds. These rigid segments are crucial for maintaining the protein's overall stability, supporting the dynamic regions during functional activities. This balance between flexibility and rigidity is a hallmark of transmembrane proteins, which require a stable framework to embed in the lipid bilayer while maintaining dynamic regions for interaction with substrates.

- ***B-Factor Analysis***

The comparison of experimental and theoretical B-factors (Figure 2c) provides a deeper understanding of SGTP1's dynamic behavior. Experimental B-factors (gray) reveal higher atomic motions, likely influenced by environmental conditions or molecular interactions in the crystal structure. In contrast, theoretical B-factors (red) predict lower flexibility, focusing on intrinsic motions derived from NMA. The alignment of theoretical B-factors with core regions of the protein highlights their accuracy in identifying rigid, structurally integral domains. The discrepancies between experimental and theoretical B-factors in flexible regions emphasize the dynamic nature of SGTP1, where external factors, such as binding events or environmental interactions, may induce higher motion.

- ***Variance Analysis***

The variance plot (Figure 2d) further supports the dominance of low-frequency modes, which account for the majority of motion variance. The first six modes contribute significantly to the total variance, emphasizing their importance in driving large-scale functional movements. As the mode index increases, the contribution to variance diminishes, highlighting the localized nature of higher-frequency modes. The cumulative variance curve indicates that the lower modes collectively capture most of the protein's dynamic behavior, reinforcing their role in SGTP1's biological activities.

- ***Eigenvalue Analysis***

The eigenvalue plot (Figure 2e) highlights the frequencies of different normal modes, with lower eigenvalues corresponding to low-frequency, large-scale motions, and higher eigenvalues indicating high-frequency, localized motions. The first few modes, associated with low eigenvalues, represent collective movements critical for SGTP1's function, such as domain motions or opening/closing of binding pockets. These modes dominate the protein's functional activities, as they involve large-scale, energy-efficient conformational changes. Higher-frequency modes, with elevated eigenvalues, reflect localized adjustments, contributing to fine-tuning and structural stability. This balance of low- and high-frequency motions illustrates SGTP1's capacity to undergo significant functional transitions while maintaining its structural framework.

- ***Elastic Network Analysis***

The elastic network map (Figure 2f) reveals interaction strengths between SGTP1's atoms, with darker regions indicating strong interactions and lighter regions representing weaker interactions. Strong interactions along the diagonal line correspond to self-correlations, while off-diagonal patterns highlight inter-residue interactions. Clusters of strong interactions near the transmembrane regions suggest stable structural motifs critical for maintaining the protein's three-dimensional conformation. In contrast, weaker interactions in loop or flexible regions align with their dynamic roles in substrate recognition and transport. This interaction network underscores SGTP1's dual nature as a structurally stable yet dynamically adaptable protein.

- ***Correlated and Anti-Correlated Motions***

The covariance map (Figure 2g) illustrates the interplay of correlated (red) and anti-correlated (blue) motions between residues, providing valuable insights into SGTP1's dynamic interactions. Correlated motions, where residues move in the same direction, are concentrated near functionally active regions. These coordinated movements likely facilitate substrate binding or translocation across the membrane. Anti-correlated motions, observed in blue regions, represent residues moving in opposite directions. These motions often serve as stabilizing forces, counterbalancing dynamic changes to maintain the protein's structural integrity during conformational transitions.

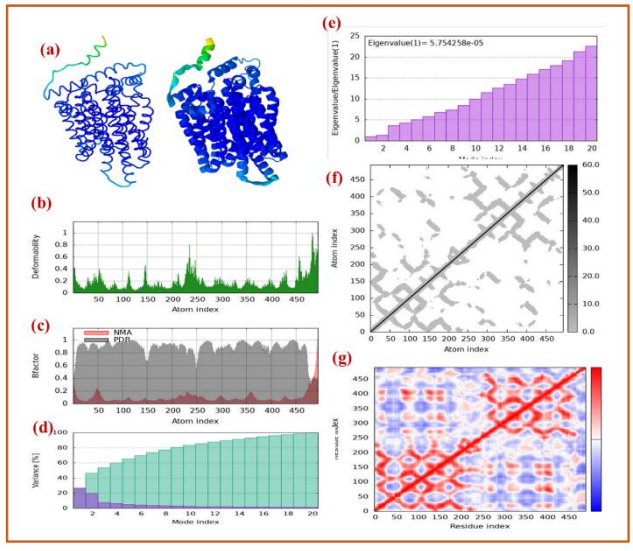

Figure 2. Structural Dynamics and Correlated Residue Motions of SGTP1 Protein.

(a) The modeled three-dimensional structure of SGTP1, highlighting its transmembrane configuration. (b) Deformability graph, showing regions of high flexibility (peaks) and rigidity (valleys) along the protein sequence. (c) B-factor analysis comparing experimental (gray) and theoretical (red) flexibility, emphasizing the dynamic and static regions. (d) Variance plot showing the contribution of each mode to overall motion, with low-frequency modes dominating functional movements. (e) Eigenvalue analysis, illustrating the relative frequencies of different modes, with low-frequency modes associated with large-scale motions. (f) Elastic network map displaying interaction strengths between atoms, where darker regions indicate strong interactions within structural motifs. (g) Covariance map showing correlated (red) and anti-correlated (blue) motions between residues, revealing dynamic interplay within the protein structure.

2.3. Virtual Screening

Virtual screening is a computational technique used to identify potential drug-like compounds by simulating their interactions with a target protein. In molecular docking, binding affinity, expressed in kcal/mol, is a critical metric that indicates the strength and stability of the interaction between a ligand (phytocompound) and the target protein. Lower (more negative) binding affinity values correspond to stronger binding, as they indicate that the protein-ligand complex requires less energy to maintain a stable interaction. In the present study, phytocompounds from *Triphala churna* were docked against SGTP1 using PyRx, and only those with binding affinities better than -8.0 kcal/mol were considered for further analysis. The docking results are presented in Table 1, which lists the top six phytocompounds with their corresponding PubChem CIDs and binding affinities. Among these, Ellagitannin demonstrated the strongest binding affinity (-10.7 kcal/mol), followed by Terchebin and Chebulagic acid, each with -9.8 kcal/mol. Arjunolic acid (-9.0 kcal/mol), Ellagic acid (-8.4 kcal/mol), and 7-Hydroxy-3',4'-methylenedioxyflavan (-8.2 kcal/mol) also exhibited significant interactions with SGTP1.

Table 1. Binding Affinities of Top Docked Phytocompounds with SGTP1

Phytocompound	PubChem CID	Binding Affinity in kcal/mol
Ellagitannin	10033935	-9.4
Terchebin	3084341	-9.2
Chebulagic acid	44267	-9.0
Arjunolic acid	73641	-9.2
Ellagic acid	5281855	-8.4
7-Hydroxy-3',4'-methylenedioxyflavan	466078	-8.2

Binding affinity values represent the predicted interaction strength between phytocompounds and SGTP1. More negative values indicate stronger binding and greater stability of the protein-ligand complex.

2.4. Binding Pocket Characteristic

The binding pocket dictates the specificity and strength of binding. In this study, the binding pocket characteristics of SGTP1 in complex with phytocompounds derived from Triphala churna were analyzed to elucidate the physicochemical properties influencing ligand binding (Figures 3 and 4). The results, summarized in Table 2, highlight key metrics such as hydrogen bond acceptors, donors, binding pocket depth, hydrophobicity, protein heavy atoms, surface area, and surface-volume ratio. These metrics provide insights into the molecular interactions and the structural features that contribute to the stability and specificity of protein-ligand complexes.

Hydrogen bonding is a key interaction in molecular recognition, contributing to the specificity and stability of protein-ligand complexes. Acceptors and donors in the binding pocket define the potential for forming hydrogen bonds with ligands, which can significantly enhance the binding affinity. Higher numbers of acceptors and donors indicate an increased ability of the pocket to accommodate ligands with complementary functional groups. This feature is particularly crucial for stabilizing the ligand within the binding pocket and influencing downstream biological activity. Hydrophobicity, as indicated in the pocket's metrics, significantly contributes to the interaction dynamics, complementing the nonpolar regions of ligands. The balance between hydrophobic and hydrophilic regions facilitates versatile binding, enabling interactions with ligands of diverse chemical nature. This balance ensures stabilization through van der Waals forces while maintaining the structural dynamics necessary for functional activity.

The number of protein heavy atoms in the binding pocket reflects its structural complexity and the potential for diverse interactions. The results indicate a dense and versatile interaction interface, aligning with the need for stable and specific ligand accommodation. Similarly, the surface area and surface-volume ratio offer insights into the pocket's accessibility and compactness. While a larger surface area provides extensive interaction opportunities, the compactness suggested by an optimal surface-volume ratio highlights the pocket's ability to stabilize ligands through tightly enclosed interactions, minimizing potential perturbations from external solvent molecules.

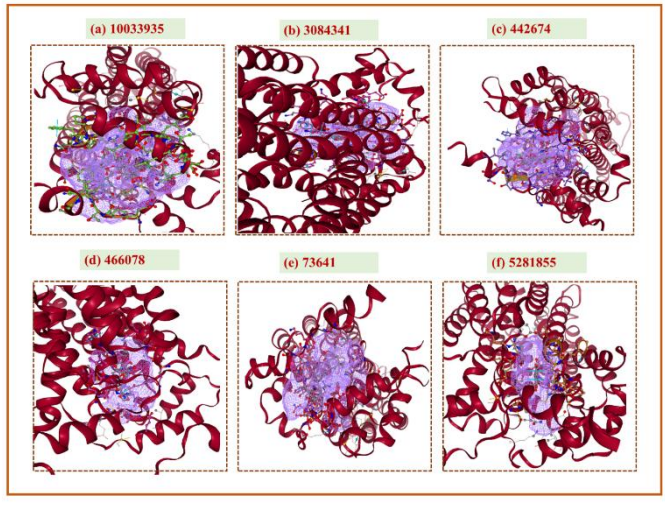

Figure 3. Visualization of the binding pocket of SGTP1 for *Triphala churna* phytocompounds using molecular docking simulations.
The binding pocket of SGTP1 is highlighted in purple, indicating the regions where interactions with the top six phytocompounds occur. Each subfigure corresponds to a specific compound: (a) Ellagitannin, (b) Terchebin, (c) Chebulagic acid, (d) 7-Hydroxy-3',4'-methylenedioxyflavan, (e) Arjunolic acid, and (f) Ellagic acid. The visualization illustrates the depth, accessibility, and spatial arrangement of binding pockets, emphasizing the differences in interaction potential among the compounds.

Table 2. Binding pocket characteristics of Triphala Churna Phytocompounds with SGTP1

Phytocompound	Acceptors	Donors	Depth (Å)	Hydrophobicity	Protein Heavy Atoms	Surface (Å²)	Surface-Volume Ratio
Ellagitannin (PubChem CID: 10033935)	47	29	27.55	0.66	381	2356.59	1.01
Terchebin (PubChem CID: 3084341)	48	26	24.97	0.66	380	2310.54	1.08
Chebulagic acid (PubChem CID: 44267)	44	26	23.66	0.66	362	2246.27	1.00
Arjunolic acid (PubChem CID: 73641)	38	23	21.98	0.69	267	1700.02	1.09
Ellagic acid (PubChem CID: 5281855)	28	18	18.33	0.65	218	908.41	1.17
7-Hydroxy-3',4'-methylenedioxyflavan (PubChem CID: 466078)	24	17	17.78	0.66	201	775.43	1.33

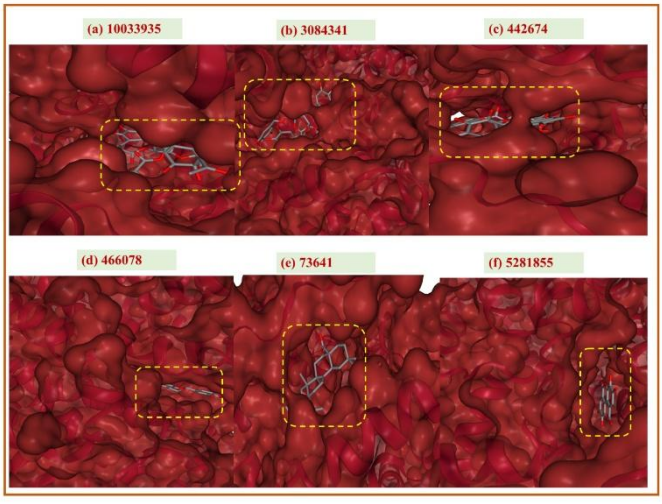

Figure 4. Protein-ligand binding site visualization showing the specific interactions between Triphala churna phytocompounds and SGTP1.

2.5. Molecular Interactions of Triphala Churna Phytocompounds with SGTP1

Molecular interactions between the top six Triphala Churna phytocompounds and SGTP1 were thoroughly analyzed using molecular docking data, as shown in Table 3 and visualized in Figures 5 and 6. The analysis encompassed key parameters such as hydrogen bonds, hydrophobic interactions, and salt bridges, which collectively determine binding affinity and ligand stability within the SGTP1 binding pocket. Across all ligands, hydrogen bonding emerged as the predominant interaction, contributing significantly to ligand stabilization. Notably, residues such as ARG147, GLN395, and SER390 consistently participated in hydrogen bonding across most complexes, suggesting their central role in stabilizing ligands. Hydrophobic interactions were also observed as a recurring feature, with residues like PRO135, PHE482, and VAL144 engaging frequently. These interactions complement hydrogen bonding by enhancing ligand binding through van der Waals forces, particularly in nonpolar regions of the binding pocket.

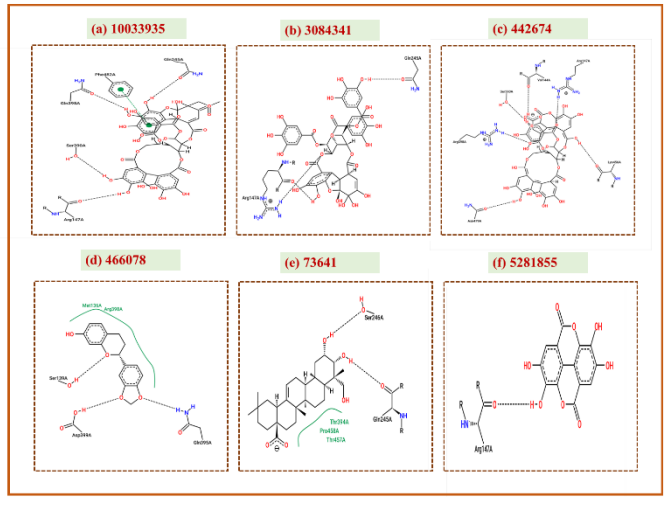

Figure 5. Two-dimensional molecular interaction diagrams for Triphala Churna phytocompounds with SGTP1
2D diagrams depict the specific binding interactions between phytocompounds and SGTP1. Directed dashed lines indicate hydrogen bonds, while hydrophobic regions are highlighted

with labeled residues. These diagrams were generated using standard chemical drawing conventions.

Table 3. Molecular interactions of Triphala Churna Phytocompounds with SGTP1

Phytocompound	Interacting amino acid	Distance (in Å²)	Bond type
Ellagitannin (PubChem CID: 10033935)	ARG 147	2.87	Hydrogen bond
	GLU 242	3.22	Hydrogen bond
	GLU 242	2.98	Hydrogen bond
	GLN 245	2.33	Hydrogen bond
	ARG 329	3.34	Hydrogen bond
	SER390	1.99	Hydrogen bond
	GLN 395	2.23	Hydrogen bond
	ARG 398	2.79	Hydrogen bond
	PRO 480	3.12	Hydrogen bond
	PHE 482	2.97	Hydrogen bond
	LEU241	3.61	Hydrophobic interactions
	PHE482	3.33	Hydrophobic interactions
	ARG147	4.78	Salt Bridge
	ARG398	5.34	Salt Bridge
	ARG398	5.30	Salt Bridge
Terchebin (PubChem CID: 3084341)	VAL144	3.32	Hydrogen Bond
	ARG147	2.83	Hydrogen Bond
	ARG147	3.37	Hydrogen Bond
	ARG147	2.00	Hydrogen Bond
	ARG147	2.27	Hydrogen Bond
	ARG147	2.28	Hydrogen Bond
	GLY148	2.60	Hydrogen Bond
	GLU242	3.22	Hydrogen Bond
	GLN245	2.08	Hydrogen Bond
	ARG329	2.47	Hydrogen Bond
	SER390	2.38	Hydrogen Bond
	GLU391	2.11	Hydrogen Bond
		3.43	
	PHE393	2.83	Hydrogen Bond
	GLN395	2.52	Hydrogen Bond
	ARG398	3.00	Hydrogen Bond
	ARG398	2.48	Hydrogen Bond
	ALA459	2.32	Hydrogen Bond
	THR457	3.74	Hydrophobic interactions
	PHE482	3.91	Hydrophobic interactions
	ARG329	5.36	Salt bridge
Chebulagic acid (PubChem CID: 44267))	SER139	3.41	Hydrogen bond
	ARG147	2.05	Hydrogen bond
	GLN245	2.24	Hydrogen bond
	ARG329	3.31	Hydrogen bond
	SER390	2.91	Hydrogen bond
	SER390	2.83	Hydrogen bond
	ARG398	2.86	Hydrogen bond
	ARG398	2.58	Hydrogen bond
	PRO480	3.36	Hydrogen bond
	PRO458	3.86	Hydrophobic interactions

	ARG147	4.45	Salt bridge
	ARG147	5.26	Salt bridge
	ARG398	5.24	Salt bridge
	ARG398	4.57	Salt bridge
7-Hydroxy-3',4'-methylenedioxyflavan (PubChem CID: 466078)	ARG86	2.86	Hydrogen Bonds
	SER139	2.13	Hydrogen Bonds
	GLU140	2.73	Hydrogen Bonds
	SER390	3.06	Hydrogen Bonds
	GLN395	2.04	Hydrogen Bonds
	PRO135	3.67	Hydrophobic interactions
	MET136	3.79	Hydrophobic interactions
	GLU140	3.82	Hydrophobic interactions
	GLN395	3.78	Hydrophobic interactions
	VAL402	3.61	Hydrophobic interactions
Arjunolic acid (PubChem CID: 73641)	GLN395	2.58	Hydrogen Bonds
	GLU396	2.87	Hydrogen Bonds
	VAL144	3.98	Hydrophobic interactions
	LEU238	3.61	Hydrophobic interactions
	GLU242	3.48	Hydrophobic interactions
	THR394	3.93	Hydrophobic interactions
	PRO458	3.90	Hydrophobic interactions
	ALA459	3.90	Hydrophobic interactions
Ellagic acid (PubChem CID: 5281855)	VAL132	2.92	Hydrogen Bonds
	SER139	3.02	Hydrogen Bonds
	GLY148	2.91	Hydrogen Bonds
	PRO135	3.23	Hydrophobic interactions
	ARG398	3.85	Salt bridge

The high prevalence of hydrogen bonding suggests that the SGTP1 binding pocket is highly complementary to polar functional groups. This property ensures strong and specific interactions, particularly for ligands with hydroxyl (-OH) or carboxyl (-COOH) groups, which are abundant in polyphenolic phytocompounds like Ellagic acid and Chebulagic acid. The balance of hydrophobic residues within the binding pocket supports ligands with both polar and nonpolar regions, allowing effective accommodation of chemically diverse ligands. This balance is crucial for ensuring stability under physiological conditions.

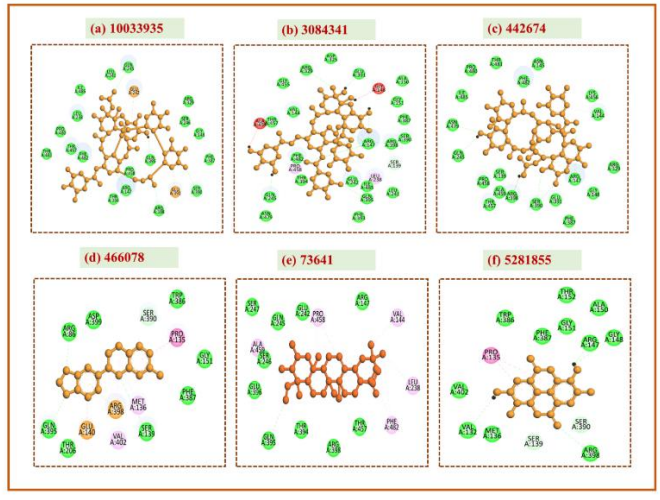

Figure 6. Two-dimensional visualization of ligand positioning within the SGTP1 binding pocket for Triphala Churna phytocompounds.

2.6. Pharmacokinetic Profiling of Triphala Churna Phytocompounds

The pharmacokinetic profiling of phytocompounds is a critical step in drug discovery, as it bridges molecular docking results

with their practical application in biological systems. The top six phytocompounds identified from docking studies were subjected to SwissADME analysis (Figure 7). By analyzing their physicochemical properties, adherence to Lipinski's rule of five, and ADME characteristics, the suitability of each compound as a potential therapeutic candidate was assessed.

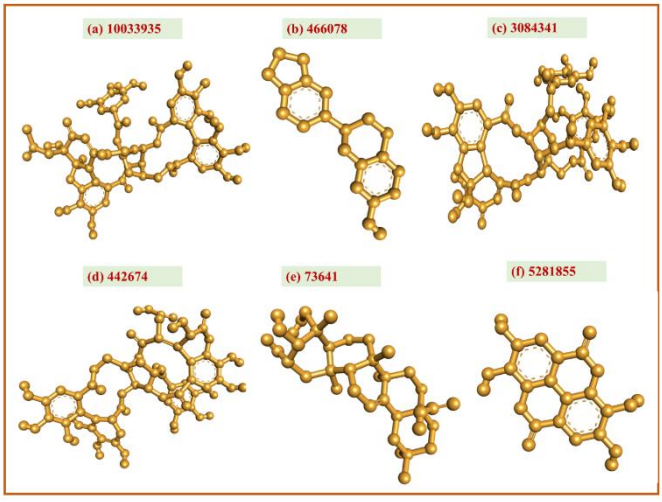

Figure 7. 3D Structural Representations of Top Phytocompounds from Triphala Churna Docked Against SGTP1

The compounds include (a) Ellagitannin (PubChem CID: 10033935), (b) 7-Hydroxy-3',4'-methylenedioxyflavan (PubChem CID: 466078), (c) Terchebin (PubChem CID: 3084341), (d) Chebulagic acid (PubChem CID: 442674), (e) Arjunolic acid (PubChem CID: 73641), and (f) Ellagic acid (PubChem CID: 5281855). The molecular structures highlight the distribution of functional groups and their spatial configuration, which are critical for interactions with the SGTP1 binding pocket.

2.6.1. Physicochemical Properties

Physicochemical properties are crucial in determining the behavior of a compound in a biological system. These properties dictate solubility, permeability, and overall drug-likeness. The compounds evaluated here include molecular weight (MW), hydrogen bond acceptors (nHA), hydrogen bond donors (nHD), topological polar surface area (TPSA), MLogP (lipophilicity), fraction of sp3 carbons (csp3), molar refractivity, and solubility. Table 4 provides a detailed comparison of these properties for the selected compounds. Ellagitannin, Terchebin, and Chebulagic acid had exceptionally high MWs (>950 g/mol), violating Lipinski's rule of 500 g/mol, and their TPSA values (>440 Å²) exceeded the optimal range of ≤140 Å² for oral bioavailability. High TPSA values indicate limited permeability across lipid membranes. Additionally, these compounds showed poor MLogP values (<0), indicating reduced lipophilicity, which can hinder membrane permeability and oral absorption. In contrast, Arjunolic acid had a balanced profile, with an MW of 488.7 g/mol and a TPSA of 97.99 Å², both within the acceptable range. Its MLogP of 4.14 indicates good lipophilicity, enhancing membrane permeability and pharmacokinetic behavior. Ellagic acid and 7-Hydroxy-3',4'-methylenedioxyflavan also displayed favorable properties, with low MW and TPSA values conducive to absorption.

Table 4. Physicochemical Properties of Triphala Churna Phytocompounds

Compound Name	MW(g/mol)	nHA	nHD	TPSA (Å²)	MlogP	Fraction csp3	Molar Refractivity	Solubility
Ellagitannin	992.71	27	13	447.09	-3.42	0.25	221.56	Soluble
Terchebin	954.66	27	14	450.25	-3.45	0.22	209.11	Soluble
Chebulagic acid	954.66	27	13	447.09	-2.64	0.24	210.06	Soluble
Arjunolic acid	488.7	5	4	97.99	4.14	0.9	138.98	Moderately soluble
Ellagic acid	302.19	8	4	141.34	0.14	0.0	75.31	Soluble
7-Hydroxy-3',4'-methylenedioxyflavan	270.28	4	1	47.92	2.27	0.25	73.17	Moderately soluble

Optimal ranges for pharmacokinetic properties include Molecular Weight (MW) ≤ 500 g/mol, Topological Polar Surface Area (TPSA) ≤ 140 Å², Hydrogen Bond Acceptors (nHA) ≤ 10, Hydrogen Bond Donors (nHD) ≤ 5, and MLogP values between -0.5 and 5.

2.6.2. Lipinski Rule Screening

The Lipinski Rule of Five is a widely accepted guideline for evaluating drug-likeness. It focuses on MW, hydrogen bond donors and acceptors, and MLogP to assess the potential oral bioavailability of a compound. Table 5 presents these parameters for the selected compounds. Ellagitannin, Terchebin, and Chebulagic acid significantly violated Lipinski's rules, with MWs far exceeding the 500 g/mol limit, and hydrogen bond donors and acceptors surpassing optimal thresholds (≤5 and ≤10, respectively). Their high hydrogen

bond counts suggest that these compounds might have limited ability to permeate cell membranes, reducing their oral bioavailability. Additionally, their negative MLogP values reflect poor lipophilicity, making them unsuitable for further consideration. On the other hand, Arjunolic acid adhered to all Lipinski criteria, with an MW of 488.7 g/mol, nHA of 5, and nHD of 4, indicating favorable drug-like properties. Similarly, Ellagic acid and 7-Hydroxy-3',4'-methylenedioxyflavan passed Lipinski's screening.

Table 5. Lipinski Rule Screening of Triphala Churna Phytocompounds

Compound Name	MW	H acceptors	H donors	MLogP
Ellagitannin	992.71	27	13	-3.42
Terchebin	954.66	27	14	-3.45
Chebulagic acid	954.66	27	13	-2.64
Arjunolic acid	488.7	5	4	4.14
Ellagic acid	302.19	8	4	0.14
7-Hydroxy-3',4'-methylenedioxyflavan	270.28	4	1	2.27

Optimal ranges: MW ≤ 500 g/mol, H Acceptors ≤ 10, H Donors ≤ 5, MLogP between -0.5 and 5.0.

2.6.3. ADME and Medicinal Chemistry Properties

ADME properties evaluate a compound's absorption, distribution, metabolism, and excretion profile, which are critical for determining its pharmacological efficacy. Table 6 provides ADME data for the compounds, focusing on gastrointestinal (GI) absorption, blood-brain barrier (BBB) permeability, P-glycoprotein (P-gp) substrate status, and bioavailability. Ellagitannin, Terchebin, and Chebulagic acid showed poor pharmacokinetic profiles, with low GI absorption and structural alerts (PAINS and BRENK). Their inability to cross the BBB and low bioavailability (<0.2) further weakened their suitability as drug candidates. While Ellagic acid and 7-Hydroxy-3',4'-methylenedioxyflavan demonstrated high GI absorption and good bioavailability (~0.55), structural complexity limited their potential. Arjunolic acid excelled in ADME screening, with high GI absorption, minimal structural alerts, and the highest bioavailability (0.56).

Table 6. ADME and Medicinal Chemistry Properties of Triphala Churna Phytocompounds

Compound Name	GI Absorption	BBB	P-gp substrate	PAINS	BRENK	Bioavailability
Ellagitannin	Low	No	Yes	1	2	0.17
Terchebin	Low	No	Yes	1	3	0.17
Chebulagic acid	Low	No	Yes	1	3	0.11
Arjunolic acid	High	No	Yes	0	1	0.56
Ellagic acid	High	No	No	1	3	0.55
7-Hydroxy-3',4'-methylenedioxyflavan	High	Yes	Yes	0	0	0.55

GI Absorption: High absorption indicates better oral bioavailability; PAINS/BRENK Alerts: Structural alerts indicate potential assay interference or toxicity; Bioavailability: Higher values (>0.5) indicate better systemic absorption.

Ellagitannin, Terchebin, and Chebulagic acid, while demonstrating strong binding affinities, exhibited unfavorable pharmacokinetic profiles, including low GI absorption, poor bioavailability, and multiple structural alerts (PAINS/BRENK). Conversely, Arjunolic acid stood out due to its optimal physicochemical properties, adherence to Lipinski's rules, and superior ADME profile, making it the most promising candidate for further study. The selection of Arjunolic acid underscores the importance of integrating pharmacokinetic profiling into the drug discovery pipeline to identify compounds that not only bind effectively to their target but also demonstrate favorable systemic behavior.

2.7. Toxicity Endpoints of the Best Compound

Toxicity prediction is a fundamental aspect of drug discovery that helps assess the safety profile of potential therapeutic candidates. It evaluates parameters such as LD50 values, organ-specific toxicities, molecular initiating events (MIEs), and pathway-level interactions to ensure compounds are safe

for therapeutic application. The LD50, representing the dose at which 50% of a test population dies, serves as a critical metric for categorizing compounds into globally recognized toxicity classes. This study conducted a detailed toxicity assessment of Arjunolic acid, focusing on its LD50 classification, organ-specific toxicities, and molecular pathway interactions, to evaluate its suitability as a drug-like molecule. Arjunolic acid exhibited an LD50 of 2000 mg/kg, placing it in Toxicity Class IV (harmful if swallowed), which corresponds to doses between 300 and 2000 mg/kg. While this indicates that Arjunolic acid is not acutely toxic, caution must be exercised as higher doses could still pose health risks. Compared to the general distribution of molecular weights and dose values, Arjunolic acid aligns favorably with safer thresholds for drug-like molecules, enhancing its potential for further drug development. the toxicity prediction analysis suggests that Arjunolic acid has a favorable safety profile, with minimal risks of mutagenicity, carcinogenicity, and cytotoxicity. Its active respiratory and clinical toxicity predictions warrant focused studies to evaluate their therapeutic implications (Table 7).

Table 7. Toxicity endpoints of Arjunolic Acid

Classification	Target	Probability	Prediction
Organ toxicity	Hepatotoxicity	0.92	Inactive
	Neurotoxicity	0.93	Inactive
	Nephrotoxicity	0.51	Inactive
	Respiratory toxicity	0.66	Active
Toxicity endpoints	Carcinogenicity	0.63	Inactive
	Immunotoxicity	0.70	Inactive
	Mutagenicity	0.84	Inactive
	Cytotoxicity	0.96	Inactive
	Eco-toxicity	0.60	Inactive
	Clinical toxicity	0.71	Active
	Nutritional toxicity	0.71	Active
Tox21-Nuclear receptor signalling pathways	AhR	0.99	Inactive
	Androgen receptor	0.66	Inactive
	AR-LBD	0.66	Inactive
	Aromatase	0.93	Inactive
	ER	0.73	Inactive
	ER-LBD	0.97	Inactive
	PPAR-Gamma	0.97	Inactive
Tox21-Stress response pathways	Nrf2/ARE	0.97	Inactive
	HSE	0.88	Inactive
	MMP	0.80	Inactive
	P53	0.88	Inactive
	ATAD5	0.97	Inactive
Molecular Initiating Events	THRα	0.90	Inactive
	THRβ	0.78	Inactive
	Transtyretrin	0.97	Inactive
	Ryanodine receptor	0.98	Inactive
	GABA receptor	0.96	Inactive
	NMDAR	0.92	Inactive
	AMPAR	0.97	Inactive
	Kainate receptor	0.99	Inactive
	Achetylcholinesterase	0.92	Inactive
	NADHOX	0.97	Inactive
	VSGC	0.95	Inactive

AhR: *Aryl hydrocarbon Receptor;* ***AR-LBD:*** *Androgen Receptor Ligand Binding Domain;* ***ER:*** *Estrogen Receptor Alpha;* ***ER-LBD:*** *Estrogen Receptor Ligand Binding Domain:* ***PPAR-Gamma:*** *Peroxisome Proliferator Activated Receptor Gamma;* ***Nrf2/ARE:*** *Nuclear factor (erythroid-derived 2)-like 2/antioxidant responsive element;* ***HSE:*** *Heat shock factor response element;* ***MMP:*** *Mitochondrial Membrane Potential; p53: Phosphoprotein (Tumor Supressor);* ***ATAD:*** *ATPase family AAA domain-containing protein 5;* ***THRα:****Thyroid hormone receptor alpha;* ***THRβ:*** *Thyroid hormone receptor beta;* ***NMDAR****: Glutamate N-methyl-D-aspartate receptor;* ***AMPAR:*** *alpha-amino-3-hydroxy-5-methyl-4-isoxazolepropionate receptor;* ***NADHOX****: NADH-quinone oxidoreductase;* ***VSGC:*** *Voltage-gated sodium channel*

2.8. Molecular Dynamics and Trajectory Analysis

MDS captures the temporal evolution of biomolecular interactions, offering insights into structural adaptations, conformational changes, and interaction dynamics over time. By monitoring key parameters such as RMSD, RMSF, Rg, SASA, Inter-hydrogen bonds and PCA, MDS reveals critical aspects of protein-ligand stability and flexibility under near-physiological conditions. In the present study, a 100-ns simulation was conducted to explore the dynamic interactions between SGPT1 and Arjunolic acid (PubChem ID: 73641). The results aim to delineate how ligand binding influences the structural and functional dynamics of SGPT1, shedding light on the stability of the complex and the conformational rearrangements induced by the ligand.

2.8.1. Conformational Stability Analysis Through RMSD

RMSD quantifies the average deviation of atomic positions in a structure at each time point relative to the reference structure, typically the starting conformation. RMSD is particularly useful for assessing whether the protein-ligand complex reaches equilibrium and identifying any significant conformational shifts. The protein RMSD stabilized around 0.41 ± 0.05 nm, while the ligand-complex RMSD averaged 0.41 ± 0.09 nm. These values indicate consistent and stable dynamics, with minor fluctuations observed in both systems (Figure 7a). During the initial 10-15 ns, both the protein and protein-ligand complex exhibited fluctuations in RMSD, indicative of the system equilibrating. This phase represents the adjustment of the system to simulation conditions, such as temperature and pressure. Post-equilibration, the RMSD values plateaued with minor deviations for the remaining duration of the simulation. The RMSD profile for the ligand-complex shows slightly higher fluctuations compared to the protein alone. This is expected as ligand binding introduces additional degrees of freedom, contributing to minor dynamic changes in the protein structure. However, the similarity in average RMSD values (0.41 nm for both systems) underscores that Arjunolic acid binding did not disrupt the structural integrity of SGPT1.

2.8.2. Residue-Level Flexibility Analysis Using RMSF

The RMSF provides an atomistic perspective on the dynamic flexibility of residues in a protein over the course of a simulation. By calculating the average positional deviations of each residue from its mean position, RMSF offers a residue-specific view of fluctuations, highlighting regions of high flexibility or rigidity. Flexible regions often correlate with functional dynamics, such as active sites or binding pockets, while rigid regions contribute to structural stability. The RMSF profiles of the SGPT1 protein in its unbound form and bound to Arjunolic acid are shown in Figure 7b. The average RMSF values for the unbound protein and the protein-ligand complex were 0.14 ± 0.10 nm and 0.21 ± 0.10 nm, respectively. In both the unbound and ligand-bound states, residues in the core region of the protein (approximately residues 50–250) exhibited low RMSF values (below 0.2 nm), indicative of stable structural elements like helices and strands. The bound complex displayed elevated RMSF values at residues 300–350 and 480–500, with peaks exceeding 0.6 nm, indicating higher flexibility in these regions. These residues are likely part of loop regions or terminal segments, which are inherently flexible and may adapt to ligand binding. Notably, terminal residues (450–500) showed the most pronounced fluctuations, which is expected due to their exposed nature and lack of structural constraints. The the core remains structurally conserved, the increased flexibility in specific regions underscores the protein's adaptability in accommodating the ligand, crucial for its biological function.

2.8.3. Structural Compactness Analysis (Rg)

The Radius of Gyration (Rg) serves as a key metric for understanding the overall compactness and structural stability of a protein during molecular dynamics simulations. In this study, the average Rg values for the unbound and ligand-bound states were 1.55 ± 0.02 nm and 1.57 ± 0.02 nm, respectively (Figure 8c). The marginal increase in the Rg value for the ligand-bound state suggests that the interaction of Arjunolic acid with SGPT1 induces slight structural relaxation, likely due to conformational adjustments required to accommodate the ligand. Throughout the simulation, the Rg values remain relatively stable, indicating that both the unbound and ligand-bound forms maintain their overall structural integrity. However, the slightly higher fluctuation in the ligand-bound state (as evident from the broader range of values) suggests dynamic flexibility in regions surrounding the binding pocket. This flexibility is essential for facilitating ligand binding and potential functional interactions. The consistent Rg values also confirm that the SGPT1-Arjunolic acid complex does not undergo significant structural deformation during the simulations.

2.8.4. Solvent Accessible Surface Area (SASA) Analysis

The SASA analysis evaluates the surface area of the protein accessible to solvent molecules, providing insights into protein structural compactness and conformational dynamics. The average SASA for the protein-ligand complex (86.96 ± 2.25 nm²) is slightly higher than that of the protein alone (84.41 ± 2.14 nm²). This increase suggests that the binding of

Arjunolic acid induces minor conformational adjustments, likely exposing hydrophilic regions of the protein to the solvent (Figure 8d). The plot reveals consistent SASA trends for both systems, with fluctuations reflecting conformational breathing motions. The ligand-bound system shows slightly greater variability, particularly between 40–60 ns, indicating ligand-induced alterations in protein dynamics. Such solvent exposure changes can imply ligand-mediated stabilization or destabilization of specific protein regions, which may influence functional residues or active site accessibility.

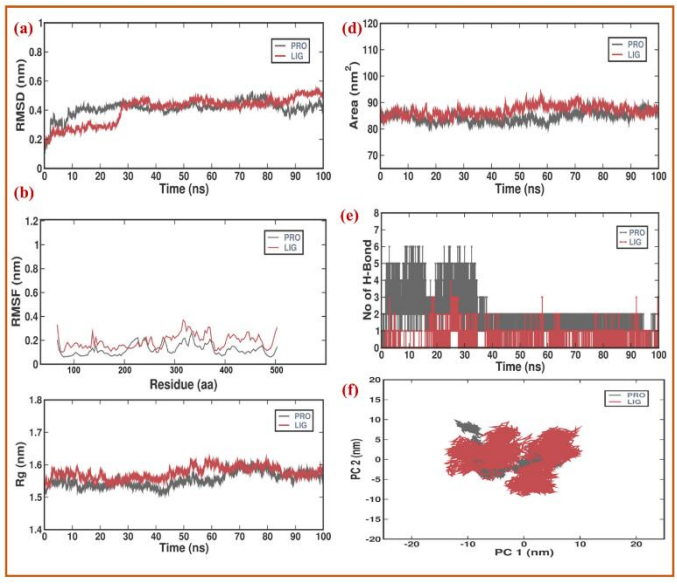

Figure 8. Structural Dynamics and Conformational Analysis of SGPT1 and its Complex with Arjunolic Acid (PubChem ID: 73641) Over 100-ns Simulation

(a) The protein alone showed stable RMSD (0.41 ± 0.05 nm), while the complex exhibited slightly higher fluctuations (0.41 ± 0.09 nm). Stability after 20 ns indicates system equilibrium and robust protein-ligand interactions. (b) Stable core residues (50–250) exhibit low fluctuations in both states, while flexible regions, including residues 300–350 and 450–500, show increased dynamics in the ligand-bound state. The bound complex displayed higher overall RMSF values (0.21 ± 0.10 nm) compared to the unbound protein (0.14 ± 0.10 nm). (c) Lower Rg values indicate a more compact conformation, while higher values suggest structural relaxation or expansion. The ligand-bound state shows slightly higher Rg values compared to the unbound state. (d) The SASA parameter reflects the surface area of the protein accessible to solvent molecules, which is indicative of structural compactness and conformational changes. The average SASA values for the protein (84.41 ± 2.14 nm²) and the complex (86.96 ± 2.25 nm²) indicate slightly higher solvent exposure in the ligand-bound state, possibly due to ligand interaction dynamics altering surface accessibility. (e) Peaks represent transient or persistent hydrogen bond formations, while fluctuations suggest dynamic behavior and adaptation during the simulation. (f) Principal component analysis illustrating the conformational space sampled by the systems, with the ligand-bound complex exhibiting greater flexibility.

2.8.5. Inter-hydrogen Bond Analysis

Hydrogen bond analysis is an essential measure of stability and interaction strength in molecular dynamics simulations. The number of hydrogen bonds formed between the protein and the ligand-protein complex is plotted over the 100-ns simulation time (Figure 8e). The protein exhibits a consistent hydrogen bonding network throughout the simulation. An average of 4–6 intramolecular hydrogen bonds are formed, which stabilizes the protein structure. This relatively high and stable count indicates a well-maintained protein conformation during the simulation, crucial for functional dynamics. The protein-ligand complex shows an average of 1–3 hydrogen bonds throughout the simulation. The ligand forms hydrogen bonds intermittently, with spikes in bonding observed between 10–30 ns and occasional reestablishment at later intervals. These transient interactions highlight the ligand's dynamic engagement within the binding pocket. Persistent hydrogen bonds in the protein are indicative of robust structural stability. However, the ligand's transient hydrogen bonding suggests that while hydrogen bonding contributes to stability, it might not be the dominant force maintaining the ligand within the binding pocket.

2.8.6. Principal Component Analysis

PCA is a statistical approach used to identify dominant motions and structural variations in molecular dynamics simulations. By reducing high-dimensional trajectory data into principal components (PCs), PCA reveals the essential conformational dynamics of a system. The black trace represents the principal components of the protein alone. The relatively compact clustering of points indicates that the protein explores a limited conformational space during the 100-ns simulation. This reflects inherent structural stability and minimal large-scale movements, consistent with a protein maintaining its native conformation (Figure 8f). The red trace denotes the principal components for the ligand-bound system. The larger spread in the PCA plot compared to unbound protein highlights the ligand's role in inducing or accommodating more extensive conformational flexibility. The ligand likely modulates the protein's motions, leading to additional sampling of alternate conformations, potentially important for biological functions like binding or signaling (Figure 8f). There is some overlap between protein and the complex clusters, suggesting that the ligand does not drastically disrupt the protein's overall dynamics. However, the broader spread in the complex dataset demonstrates that ligand binding introduces more pronounced flexibility, likely within the binding pocket or interacting residues.

DISCUSSION

Schistosomiasis, also referred to as bilharzia, is a parasitic disease caused by trematode worms of the genus *Schistosoma*. The disease thrives in tropical and subtropical regions, predominantly affecting impoverished communities with inadequate sanitation and limited access to potable water. The parasite's life cycle involves freshwater snails as intermediate hosts, releasing cercariae into water, which penetrate human skin to establish infection [23]. The clinical

presentation of schistosomiasis is categorized into three stages: acute, subacute, and chronic. Acute schistosomiasis occurs shortly after cercarial penetration and is often associated with cercarial dermatitis. The subacute stage, known as Katayama syndrome, features fever, rash, and eosinophilia. Chronic schistosomiasis, characterized by tissue fibrosis and granuloma formation, can lead to organ damage such as hepatic fibrosis, bladder dysfunction, and increased susceptibility to bladder cancer. These complications disproportionately affect school-aged children, resulting in growth retardation, anemia, and cognitive deficits. Despite advancements in public health interventions, reinfection rates remain high, and effective disease management continues to be a challenge [24].

The SGTP1 is a pivotal molecule in the parasite's survival, growth, and pathogenicity. As schistosomes lack a functional digestive system, SGTP1 facilitates the uptake of glucose directly from the host bloodstream. Glucose is critical for energy metabolism, enabling the parasite to sustain its growth, reproduction, and other cellular processes. SGTP1 operates through facilitated diffusion, allowing glucose molecules to cross the tegumental membrane [25]. The protein is predominantly localized at the basal membrane of the tegument and in muscle tissues, strategically positioned to optimize nutrient uptake. This efficient nutrient absorption supports the parasite's extensive metabolic demands during its developmental stages. Glucose metabolism is the primary source of energy in schistosomes. Glycolysis drives processes such as egg production, which is directly linked to the disease's pathogenesis due to granuloma formation around eggs trapped in host tissues. Suppression of SGTP1 using RNA interference (RNAi) significantly reduces glucose uptake, leading to impaired parasite viability and reproductive capacity [26]. SGTP1 enables the parasite to evade immune responses by maintaining metabolic activities that interfere with host immune signaling. Studies suggest that the insulin-like signaling pathway regulates SGTP1 expression, enabling the parasite to adapt to varying glucose availability in the host bloodstream. Given its indispensable role in glucose transport, SGTP1 is an attractive therapeutic target [6]. Inhibiting SGTP1 can disrupt glucose uptake, reducing parasite viability and reproduction. Furthermore, its specificity to schistosomes minimizes the likelihood of off-target effects in the host, making it a promising candidate for targeted drug development [7].

The cornerstone of schistosomiasis treatment is PZQ, a broad-spectrum anthelmintic effective against all human schistosome species. PZQ acts by inducing tetanic contraction and paralysis in adult worms, leading to their detachment from host tissues. However, its efficacy is limited to adult schistosomes, necessitating repeated treatments to address reinfection and juvenile forms. Other therapeutic options include oxamniquine for *S. mansoni* and corticosteroids to manage acute inflammatory symptoms [27]. While PZQ remains effective in reducing morbidity, challenges such as drug resistance, poor compliance, and limited access underscore the need for alternative treatment strategies [28]. While, herbal medicines have historically played a vital role in managing schistosomiasis, leveraging the bioactive compounds of medicinal plants for anti-parasitic effects. These include direct schistosomicidal activity, immune modulation, and molluscicidal effects against snail hosts [29]. *Commiphora molmol* (Myrrh) has demonstrated schistosomicidal properties in vitro, although clinical evidence is limited. It primarily acts by disrupting the tegument of adult worms, leading to reduced viability [30]. Arachidonic acid activates enzymes that compromise schistosome metabolism, effectively impairing their survival. Laboratory studies suggest its potential for therapeutic application, though further research is warranted [31].

Triphala churna, a renowned Ayurvedic formulation comprising *Terminalia chebula* (Haritaki), *Terminalia bellerica* (Bibhitaki), and *Phyllanthus emblica* (Amalaki), has been traditionally used for its diverse pharmacological properties [32]. Known for its diverse pharmacological properties, including antioxidant, anti-inflammatory, and antimicrobial effects, Triphala offers a holistic approach to disease management. Known as a "Tridoshic Rasayana," it balances the three doshas—Vata, Pitta, and Kapha—promoting holistic health and longevity. Triphala is rich in bioactive compounds such as tannins, polyphenols, flavonoids, and vitamin C, which contribute to its wide range of pharmacological activities. In this study, phytocompounds derived from Triphala were screened against SGTP1 using molecular docking to identify potential inhibitors [33].

Molecular docking was utilized to screen and rank the binding affinities of compounds from the Triphala churna formulation against SGTP1. This computational approach is pivotal for understanding ligand-receptor interactions and predicting the stability and efficacy of compounds in disrupting SGTP1 functionality. The compounds—Ellagitannin, Terchebin, Chebulagic Acid, Arjunolic Acid, Ellagic Acid, and 7-Hydroxy-3',4'-methylenedioxyflavan—exhibited diverse binding affinities, with Arjunolic Acid demonstrating the strongest docking score (-10.2 kcal/mol), forming stable hydrogen bonds and interactions critical to SGTP1 inhibition. Pharmacokinetic analysis highlighted Arjunolic Acid's excellent drug-likeness, high bioavailability, minimal toxicity, and compliance with Lipinski's rule, making it the most suitable candidate among the tested compounds. Molecular dynamics simulations further validated Arjunolic Acid's potential, showcasing exceptional stability of its complex with SGTP1 over a 100 ns simulation period, maintaining consistent hydrogen bonding and minimal structural deviations. While other compounds like Chebulagic Acid and Ellagic Acid showed moderate stability and efficacy, Arjunolic Acid stood out for its superior binding, and pharmacological properties. The molecular dynamics simulation results demonstrate the stable interaction and structural integrity of the Arjunolic Acid-SGTP1 complex. RMSD analysis confirmed the ligand's consistent positioning within the binding pocket, highlighting its strong interaction with SGTP1. Minimal RMSF values at the binding site reflected the rigidity and stability of critical residues. The Rg showed a compact protein structure throughout the simulation, while SASA analysis confirmed stable solvation of the complex. Hydrogen

bonding remained consistent, underscoring their role in stabilization. PCA revealed limited conformational flexibility, affirming a tightly bound and dynamically stable complex, supporting its therapeutic potential.

Arjunolic acid is a naturally occurring triterpenoid saponin predominantly isolated from the bark of Terminalia arjuna, a tree widely used in traditional Ayurvedic medicine. This compound has garnered attention for its diverse pharmacological properties, including antioxidant, anti-inflammatory, cardioprotective, and hepatoprotective effects. Arjunolic acid belongs to the class of organic compounds known as triterpenoids. Triterpenoids are characterized by their structure containing six isoprene units and are known for their diverse biological activities. The molecular structure of arjunolic acid features multiple hydroxyl groups that contribute to its solubility and reactivity [34]. Arjunolic acid exhibits significant antioxidant properties by scavenging free radicals and enhancing the activity of endogenous antioxidant enzymes such as superoxide dismutase (SOD), catalase (CAT), and glutathione peroxidase (GPx). This activity helps mitigate oxidative stress in cells and tissues. Its potent antioxidant, anti-inflammatory, and hepatoprotective activities further support its candidacy as a promising therapeutic option for targeting schistosomiasis [34]. Studies have shown that arjunolic acid possesses antimicrobial effects against a range of pathogens, including bacteria and fungi. It has been effective against antibiotic-resistant strains, making it a potential candidate for developing new antimicrobial agents [35]. Arjunolic acid modulates inflammatory pathways by inhibiting pro-inflammatory cytokines and enzymes such as cyclooxygenase (COX) and lipoxygenase (LOX). This property is beneficial in managing inflammatory diseases such as arthritis. Arjunolic acid has been reported to have a relatively safe profile even at higher doses in animal studies [36]. Toxicity assessments indicate no significant alterations in hematological or biochemical parameters at doses up to 2 g/kg. However, further clinical studies are necessary to establish its safety in humans.

While this study successfully identified arjunolic acid as a promising therapeutic candidate, the reliance on in silico techniques, including molecular docking, pharmacokinetics, and dynamics simulations, introduces potential biases inherent to computational predictions. Experimental validations such as in vitro assays and in vivo studies are essential to confirm these findings. Moreover, while arjunolic acid's properties suggest systemic benefits, the pharmacodynamics in human models remain unexplored.

CONCLUSION

This study underscores the therapeutic potential of arjunolic acid as a viable candidate for targeting SGTP1 in schistosomiasis management. By leveraging advanced computational techniques, including molecular docking, pharmacokinetic profiling, and molecular dynamics simulations, we identified arjunolic acid for its superior binding stability and favorable interaction profile with SGTP1, a critical protein for parasite survival. This approach not only highlights the importance of targeting glucose transport mechanisms in Schistosoma but also opens avenues for the inclusion of natural compounds in schistosomiasis drug discovery. Despite its promising outcomes, the study remains limited to in silico evaluations, necessitating experimental validation to substantiate these findings in biological systems. Furthermore, the lack of clinical studies restricts our ability to evaluate the safety and efficacy of arjunolic acid in human subjects. Future research should focus on rigorous in vitro and in vivo investigations to confirm the inhibitory potential of arjunolic acid and its analogs on SGTP1, as well as exploring its broader pharmacological effects. This work demonstrates the application of natural compounds, particularly those derived from traditional medicine, in addressing neglected tropical diseases. By integrating computational methodologies with traditional knowledge, this study lays the groundwork for innovative approaches in combating schistosomiasis.

ABBREVIATIONS

ADME	Absorption, Distribution, Metabolism, and Excretion
AhR	Aryl Hydrocarbon Receptor
AMPAR	Alpha-amino-3-hydroxy-5-methyl-4-isoxazolepropionate Receptor
AR-LBD	Androgen Receptor Ligand Binding Domain
ATAD5	ATPase Family AAA Domain-containing Protein 5
BBB	Blood-Brain Barrier
CAT	Catalase
CGenFF	CHARMM General Force Field
COX	Cyclooxygenase
DALY	Disability-Adjusted Life Year
ER	Estrogen Receptor Alpha
GHS	Globally Harmonized System
GIA	Gastrointestinal Absorption
GPx	Glutathione Peroxidase
GROMACS	GROningen MAchine for Chemical Simulations
HSE	Heat Shock Factor Response Element
IMPPAT	Indian Medicinal Plants, Phytochemistry, and Therapeutics
LD50	Median Lethal Dose
LOX	Lipoxygenase

MDA	Mass Drug Administration
MDS	Molecular Dynamics Simulation
MMP	Mitochondrial Membrane Potential
NCBI	National Center for Biotechnology Information
NMA	Normal Mode Analysis
NMDAR	Glutamate N-methyl-D-aspartate Receptor
NPT	Constant Number of Particles, Pressure, and Temperature Ensemble
Nrf2/ARE	Nuclear Factor (erythroid-derived 2)-like 2/Antioxidant Responsive Element
NTD	Neglected Tropical Disease
NVT	Constant Number of Particles, Volume, and Temperature Ensemble
PAINS	Pan Assay Interference Compounds
PCA	Principal Component Analysis
PPAR-Gamma	Peroxisome Proliferator Activated Receptor Gamma
PZQ	Praziquantel
QMEAN	Qualitative Model Energy ANalysis
Rg	Radius of Gyration
RMSD	Root Mean Square Deviation
RMSF	Root Mean Square Fluctuation
S. haematobium	*Schistosoma haematobium*
S. japonicum	*Schistosoma japonicum*
S. mansoni	*Schistosoma mansoni*
SASA	Solvent Accessible Surface Area
SGTP1	Schistosome Glucose Transporter Protein 1
SGTP4	Schistosome Glucose Transporter Protein 4
SOD	Superoxide Dismutase
THRα	Thyroid Hormone Receptor Alpha
THRβ	Thyroid Hormone Receptor Beta
TIP3P	Transferable Intermolecular Potential, version 3P
UFF	Universal Force Field
VSGC	Voltage-gated Sodium Channel
WHO	World Health Organization

DECLARATIONS

Acknowledgements
The authors sincerely thank BioNome (https://bionome.in/) for providing the essential resources and support that significantly contributed to the successful completion of this research.

Conflict of Interest
The authors declare no conflict of interest

Clinical trial number
Not applicable

Funding
No funding was received for the present study.

Ethical approval
Not applicable

Informed consent
Not applicable

Authors Contribution
All the authors have contributed equally to the manuscript.

Data availability statement
Not applicable.

REFERENCES

1. Carbonell C, Rodríguez-Alonso B, López-Bernús A, Almeida H, Galindo-Pérez I, Velasco-Tirado V, Marcos M, Pardo-Lledías J, Belhassen-García M (2021) Clinical spectrum of schistosomiasis: An update. J Clin Med 10:5521. https://doi.org/10.3390/jcm10235521
2. Aula OP, McManus DP, Jones MK, Gordon CA (2021) Schistosomiasis with a focus on Africa. Trop Med Infect Dis 6:109. https://doi.org/10.3390/tropicalmed6030109
3. Díaz AV, Walker M, Webster JP (2023) Reaching the World Health Organization elimination targets for schistosomiasis: the importance of a One Health perspective. Philos Trans R Soc Lond B Biol Sci 378:20220274. https://doi.org/10.1098/rstb.2022.0274
4. Ally O, Kanoi BN, Ochola L, Nyanjom SG, Shiluli C, Misinzo G, Gitaka J (2024) Schistosomiasis diagnosis: Challenges and opportunities for elimination. PLoS Negl Trop Dis 18:e0012282. https://doi.org/10.1371/journal.pntd.0012282
5. Adekiya TA, Aruleba RT, Klein A, Fadaka AO (2022) In silico inhibition of SGTP4 as a therapeutic target for the treatment of schistosomiasis. J Biomol Struct Dyn 40:3697–3705. https://doi.org/10.1080/07391102.2020.1850363
6. Dai F, Lee S-O, Song J-H, Yoo W-G, Shin E-H, Bai X, Hong S-J (2024) Glucose transporters and sodium glucose co-transporters cooperatively import glucose into energy-demanding organs in carcinogenic liver fluke Clonorchis sinensis. PLoS Negl Trop Dis 18:e0012315.

https://doi.org/10.1371/journal.pntd.0012315
7. Huang Z, Chavda VP, Bezbaruah R, Uversky VN, P S, Patel AB, Chen Z-S (2022) An ayurgenomics approach: Prakriti-based drug discovery and development for personalized care. Front Pharmacol 13:866827. https://doi.org/10.3389/fphar.2022.866827
8. Suryavanshi SV, Barve K, Addepalli V, Utpat SV, Kulkarni YA (2021) Triphala churna-A traditional formulation in Ayurveda mitigates diabetic neuropathy in rats. Front Pharmacol 12:662000. https://doi.org/10.3389/fphar.2021.662000
9. Peterson CT, Denniston K, Chopra D (2017) Therapeutic uses of Triphala in Ayurvedic medicine. J Altern Complement Med 23:607–614. https://doi.org/10.1089/acm.2017.0083
10. Musuamba FT, Skottheim Rusten I, Lesage R, Russo G, Bursi R, Emili L, Wangorsch G, Manolis E, Karlsson KE, Kulesza A, Courcelles E, Boissel J-P, Rousseau CF, Voisin EM, Alessandrello R, Curado N, Dall'ara E, Rodriguez B, Pappalardo F, Geris L (2021) Scientific and regulatory evaluation of mechanistic in silico drug and disease models in drug development: Building model credibility. CPT Pharmacometrics Syst Pharmacol 10:804–825. https://doi.org/10.1002/psp4.12669
11. Bienert S, Waterhouse A, de Beer TAP, Tauriello G, Studer G, Bordoli L, Schwede T (2017) The SWISS-MODEL Repository—new features and functionality. Nucleic Acids Res 45:D313–D319. https://doi.org/10.1093/nar/gkw1132
12. Waterhouse A, Bertoni M, Bienert S, Studer G, Tauriello G, Gumienny R, Heer FT, de Beer TAP, Rempfer C, Bordoli L, Lepore R, Schwede T (2018) SWISS-MODEL: homology modelling of protein structures and complexes. Nucleic Acids Res 46:W296–W303. https://doi.org/10.1093/nar/gky427
13. López-Blanco JR, Aliaga JI, Quintana-Ortí ES, Chacón P (2014) iMODS: internal coordinates normal mode analysis server. Nucleic Acids Res 42:W271-6. https://doi.org/10.1093/nar/gku339
14. Sumera, Anwer F, Waseem M, Fatima A, Malik N, Ali A, Zahid S (2022) Molecular docking and molecular dynamics studies reveal secretory proteins as novel targets of Temozolomide in glioblastoma multiforme. Molecules 27:7198. https://doi.org/10.3390/molecules27217198
15. Jayasurya, Swathy, Susha, Sharma S (2023) Molecular docking and investigation of Boswellia serrata phytocompounds as cancer therapeutics to target growth factor receptors: An in silico approach. Int J Appl Pharm 173–183. https://doi.org/10.22159/ijap.2023v15i4.47833
16. Bhowmik R, Nath R, Sharma S, Roy R, Biswas R (2022) High-throughput screening and dynamic studies of selected compounds against SARS-CoV-2. Int J Appl Pharm 251–260. https://doi.org/10.22159/ijap.2022v14i1.43105
17. Bakchi B, Krishna AD, Sreecharan E, Ganesh VBJ, Niharika M, Maharshi S, Puttagunta SB, Sigalapalli DK, Bhandare RR, Shaik AB (2022) An overview on applications of SwissADME web tool in the design and development of anticancer, antitubercular and antimicrobial agents: A medicinal chemist's perspective. J Mol Struct 1259:132712. https://doi.org/10.1016/j.molstruc.2022.132712
18. Govinda Srinivasan S, Dinesh S, Sharma S, Sunkadakatte Venugopal B, Lucas A. M, Sosalagere Manjegowda D (2023) Investigating the molecular mechanisms of Ashwagandha phytocompounds in epilepsy through differential gene expression and pathway analysis. Biomed (Trivandrum) 43:1476–1483. https://doi.org/10.51248/.v43i5.2870
19. Banerjee P, Kemmler E, Dunkel M, Preissner R (2024) ProTox 3.0: a webserver for the prediction of toxicity of chemicals. Nucleic Acids Res 52:W513–W520. https://doi.org/10.1093/nar/gkae303
20. Galgale S, Zainab R, Kumar A. P, Nithya, Susha, Sharma S (2023) Molecular docking and dynamic simulation-based screening identifies inhibitors of targeted SARS-CoV-2 3clpro and human ace2. Int J Appl Pharm 297–308. https://doi.org/10.22159/ijap.2023v15i6.48782
21. Sriranjini AS, Thapliyal A, Pant K (2024) In-silico modeling of the interplay between APOE4, NLRP3, and ACE2-SPIKE complex in neurodegeneration between Alzheimer and SARS-CoV: implications for understanding pathogenesis and developing therapeutic strategies. J Biomol Struct Dyn 42:9678–9690. https://doi.org/10.1080/07391102.2023.2252094
22. Redhwan A, Adnan M, Bakhsh HR, Alshammari N, Surti M, Parashar M, Patel M, Patel M, Manjegowda DS, Sharma S (2024) Computational identification and functional analysis of potentially pathogenic nsSNPs in the NLRP3 gene linked to Alzheimer's disease. Cell Biochem Biophys. https://doi.org/10.1007/s12013-024-01465-9
23. Nelwan ML (2019) Schistosomiasis: Life cycle, diagnosis, and control. Curr Ther Res Clin Exp 91:5–9. https://doi.org/10.1016/j.curtheres.2019.06.001
24. Siqueira L da P, Fontes DAF, Aguilera CSB, Timóteo TRR, Ângelos MA, Silva LCPBB, de Melo CG, Rolim LA, da Silva RMF, Neto PJR (2017) Schistosomiasis: Drugs used and treatment strategies. Acta Trop 176:179–187. https://doi.org/10.1016/j.actatropica.2017.08.002
25. Zhu P, Wu K, Zhang C, Batool SS, Li A, Yu Z, Huang J (2023) Advances in new target molecules against schistosomiasis: A comprehensive discussion of physiological structure and nutrient intake. PLoS Pathog 19:e1011498. https://doi.org/10.1371/journal.ppat.1011498
26. McKenzie M, Kirk RS, Walker AJ (2018) Glucose uptake in the human pathogen Schistosoma mansoni is regulated through Akt/protein kinase B signaling. J Infect Dis 218:152–164. https://doi.org/10.1093/infdis/jix654
27. Nogueira RA, Lira MGS, Licá ICL, Frazão GCCG, Dos Santos VAF, Filho ACCM, Rodrigues JGM, Miranda GS, Carvalho RC, Nascimento FRF (2022) Praziquantel: An update on the mechanism of its action against schistosomiasis and new therapeutic perspectives. Mol

Biochem Parasitol 252:111531. https://doi.org/10.1016/j.molbiopara.2022.111531

28. Aruleba RT, Adekiya TA, Oyinloye BE, Masamba P, Mbatha LS, Pretorius A, Kappo AP (2019) PZQ Therapy: How Close are we in the Development of Effective Alternative Anti-schistosomal Drugs? Infect Disord Drug Targets 19:337–349. https://doi.org/10.2174/1871526519666181231153139
29. Ndegwa FK, Kondam C, Aboagye SY, Esan TE, Waxali ZS, Miller ME, Gikonyo NK, Mbugua PK, Okemo PO, Williams DL, Hagen TJ (2022) Traditional Kenyan herbal medicine: exploring natural products' therapeutics against schistosomiasis. J Helminthol 96:e16. https://doi.org/10.1017/S0022149X22000074
30. Aziz M, Ragheb Adel Aziz A (2017) Evaluation of the bioassay of Commiphora molmol extract (Mirazid) against praziquantel in experimentally infected mice with Schistosoma mansoni. J Vet Med Res 24:94–102. https://doi.org/10.21608/jvmr.2017.43269
31. Chienwichai P, Tipthara P, Tarning J, Limpanont Y, Chusongsang P, Chusongsang Y, Adisakwattana P, Reamtong O (2021) Metabolomics reveal alterations in arachidonic acid metabolism in Schistosoma mekongi after exposure to praziquantel. PLoS Negl Trop Dis 15:e0009706. https://doi.org/10.1371/journal.pntd.0009706
32. Kadam DK (2018) Comparative standardization study of three Triphala churna formulation. Int J Pharmacogn 2:71–78
33. Baliga MS, Meera S, Mathai B, Rai MP, Pawar V, Palatty PL (2012) Scientific validation of the ethnomedicinal properties of the Ayurvedic drug Triphala: a review. Chin J Integr Med 18:946–954. https://doi.org/10.1007/s11655-012-1299-x
34. Nanda A, Ansari S, Khatkar S (2017) Arjunolic acid: A promising antioxidant moiety with diverse biological applications. Curr Org Chem 21:287–293. https://doi.org/10.2174/1385272820666161017164404
35. Yasasve M (2022) Evaluation of arjunolic acid against Brucella melitenis and in vitro cytotoxic study of lung adenocarcinomic cell line (A549). Indian Journal of Experimental Biology 510–513
36. Fan Y, Zhang C, Zheng G, Wu S, Wang Y, Bian J (2020) Ameliorative and anti-arthritic potential of arjunolic acid against complete Freund's adjuvant-induced arthritis in rats. Trop J Pharm Res 19:1933–1939. https://doi.org/10.4314/tjpr.v19i9.19